J Mol Med (2013) 91:749–758
DOI 10.1007/s00109-013-0996-2

JMolMed

ORIGINAL ARTICLE

Dichloroacetate reverses the hypoxic adaptation to bevacizumab and enhances its antitumor effects in mouse xenografts

Krishan Kumar · Simon Wigfield · Harriet E. Gee · Cecilia M. Devlin · Dean Singleton · Ji-Liang Li · Francesca Buffa · Melanie Huffman · Anthony L. Sinn · Jayne Silver · Helen Turley · Russell Leek · Adrian L. Harris · Mircea Ivan

Received: 7 November 2012 / Revised: 20 December 2012 / Accepted: 2 January 2013 / Published online: 30 January 2013

Abstract Inhibition of vascular endothelial growth factor increases response rates to chemotherapy and progression-free survival in glioblastoma. However, resistance invariably occurs, prompting the urgent need for identification of synergizing agents. One possible strategy is to understand tumor adaptation to microenvironmental changes induced by antiangiogenic drugs and test agents that exploit this process. We used an in vivo glioblastoma-derived xenograft model of tumor escape in presence of continuous treatment with bevacizumab. U87-MG or U118-MG cells were subcutaneously implanted into either BALB/c SCID or athymic nude mice. Bevacizumab was given by intraperitoneal injection every 3 days (2.5 mg/kg/dose) and/or dichloroacetate (DCA) was administered by oral gavage twice daily (50 mg/kg/dose) when tumor volumes reached 0.3 cm^3 and continued until tumors reached approximately 1.5–2.0 cm^3. Microarray analysis of resistant U87 tumors revealed coordinated changes at the level of metabolic genes, in particular, a widening gap between glycolysis and mitochondrial respiration. There was a highly significant difference between U87-MG-implanted athymic nude mice 1 week after drug treatment. By 2 weeks of treatment, bevacizumab and DCA together dramatically blocked tumor growth compared to either drug alone. Similar results were seen in athymic nude mice implanted with U118-MG cells. We demonstrate for the first time that reversal of the bevacizumab-induced shift in metabolism using DCA is detrimental to neoplastic growth in vivo. As DCA is viewed as a promising agent targeting tumor metabolism, our data establish the timely proof of concept that combining it with antiangiogenic therapy represents a potent antineoplastic strategy.

Keywords Dichloroacetate · Hypoxia · Bevacizumab · Oxidative phosphorylation · Glycolysis

Krishan Kumar and Simon Wigfield are equal first authors.

Adrian L. Harris and Mircea Ivan are equal senior authors.

Electronic supplementary material The online version of this article (doi:10.1007/s00109-013-0996-2) contains supplementary material, which is available to authorized users.

K. Kumar · C. M. Devlin · M. Huffman
Department of Medicine, Indiana University, Indianapolis, IN 46202, USA

S. Wigfield · H. E. Gee · D. Singleton · J.-L. Li · F. Buffa · H. Turley · R. Leek · A. L. Harris (✉)
Department of Oncology, Weatherall Institute of Molecular Medicine, University of Oxford, John Radcliffe Hospital, Oxford OX3 9DS, UK
e-mail: adrian.harris@oncology.ox.ac.uk

A. L. Sinn · J. Silver
In Vivo Therapeutics Core,
Indiana University, Indianapolis, IN 46202, USA

M. Ivan (✉)
Department of Medicine, Immunology and Microbiology, Indiana University, 980W. Walnut Street, Room C225, Indianapolis, IN 46202, USA
e-mail: mivan@iu.edu

H. E. Gee
Department of Radiation Oncology, Sydney Cancer Centre, Royal Prince Alfred Hospital, Camperdown, New South Wales 2050, Australia

Introduction

Molecular therapies targeting neo-angiogenesis and, in particular, vascular endothelial growth factor (VEGF) have shown

antitumor activity in a variety of clinical contexts [1]. Glioblastoma (GBM) is a highly vascularized and lethal primary brain tumor, with median survival of approximately 12–14 months, and therefore, represents an important target for antiangiogenic drugs [2]. Bevacizumab, a humanized anti-VEGF antibody, is currently approved by the Food and Drug Administration as a second-line treatment of GBM, and ongoing clinical trials aim at assessing its potential as a first-line agent [3]. However, as VEGF blockade prolongs progression-free survival but not overall survival, it is imperative to identify strategies that increase its impact and delay the onset of resistance [4]. For example, limited progress has been achieved in combination with irinotecan; however, no impact on overall survival could be demonstrated [5]. One major limitation in developing synergistic combinations centered on anti-VEGF agents is lack of robust clinical data as tumors that are becoming resistant to these agents are not routinely available for further analyses. Moreover, the cellular and molecular consequences of anti-VEGF treatment are still insufficiently understood. Detailed information at the molecular level on how bevacizumab affects GBM during an extended timeframe is not only essential to our understanding of tumor adaptive responses and subsequent treatment failure but also to the development of rational combination therapies.

We, therefore, sought to determine the tumor response to bevacizumab at the phenotypic and molecular level in xenograft models derived from GBM cell lines. By extending the models until eventual therapeutic failure despite continuous bevacizumab treatment, we aimed to capture the tumor adaptive programs and the corresponding rewiring of the molecular pathways using microarray analysis. We hypothesized that the core mechanisms of resistance would be reflected in alteration of these pathways, and small molecules which interfere with these processes represent realistic candidates to increase the potency of bevacizumab. Bioinformatic analysis revealed that resistant tumors exhibit a strong hypoxia-inducible factor (HIF) signature and shift from mitochondrial respiration to glycolysis. Reactivation of mitochondrial respiration with the orphan drug dichloroacetate (DCA) enhances the transient effect of bevacizumab, in contrast to the lack of additive effect of 2-deoxyglucose (2-DG), which primarily targets glycolysis. Our data provide insights into the plasticity of tumor metabolism in response to therapeutic challenges and suggest novel opportunities for synergistic interventions.

Materials and methods

In vivo tumorigenicity

All protocols were carried out under Indiana University Institutional Animal Care and Use Committee, and UK Home Office approved protocols and regulations. 10^7 U87-MG cells (purchased from ATCC) were implanted into 6- to 8-week-old female BALB/c SCID mice (Harlan Sprague Dawley, Inc.) subcutaneously, as 100-μL cell suspensions with an equal volume of Matrigel (BD Bioscience). Tumors were measured twice a week with a caliper, and volumes were calculated using the formula length × width × height × 0.52. Once the tumor volume reached 150 mm^3, mice were randomized into two groups with starting cohort sizes of five mice per group and treatment of bevacizumab (Roche) injected intraperitoneally every 3 days at a dose of 10 mg/kg or saline control begun. Treatment was continued until tumors grew to approximately a volume of 600–800 mm^3 at which point the mice were euthanized and tumors were surgically excised quickly. For the athymic nude mice xenograft models, either U87-MG cells were implanted as above into 4- to 8-week-old female mice (Harlan Laboratories, Indianapolis, IN, USA), or 7×10^6 U118-MG cells (purchased from ATCC) were grafted. Tumor fragments were either processed by formalin fixation before paraffin embedding for IHC or frozen for later RNA extraction, as described previously [6].

Drug delivery protocols for combination studies

DCA was administered by oral gavage twice daily at 50 mg/kg/dose in sterile water (vehicle control was sterile water). This dose was based on published reports and allometric scaling. Thus, 100 mg/kg per mouse per day translates into approximately 13 mg/kg in humans (http://home.fuse.net/clymer/minor/allometry.html), which is consistent with the doses used in clinical settings. Bevacizumab was given intraperitoneally at a concentration of 2.5 mg/kg/dose (U87-MG) or 2.0 mg/kg/dose (U118-MG). Treatment was continued until tumors grew to approximately 20 mm in diameter at which point the mice were euthanized and tumors quickly excised. 2-Deoxyglucose (Sigma, 500 mg/kg) was delivered via intraperitoneal injection daily.

The details of cell culture, gene array analysis, histological analysis and immunohistochemistry, DCA-treated spheroids, and RNA isolation and quantitative RT-PCR (QPCR) analysis are described in the Electronic supplementary material.

Statistical analysis

Statistical significance of observed differences among different experimental groups was calculated using a two-tailed t test. P values <0.05 were considered to be statistically significant.

Results

Establishment of the bevacizumab-resistance tumor model

U87-MG cell suspensions were subcutaneously injected into the right flank of SCID mice. Treatment with bevacizumab

(intraperitoneal injection of 10 mg/kg every 3 days) was initiated when tumors averaged 100–200 mm^3. Divergence between the treated and non-treated cohorts was evident 1 week later, and at approximately day 40, complete resistance to bevacizumab was achieved (Fig. 1). Tumors were excised separately for controls and treated cohorts at time points when their average growth rates and sizes were similar. An analogous response (i.e., initial response followed by resistance) was observed using a submaximal dose of bevacizumab (2.5 mg/kg; every 3 days by intraperitoneal injection) in athymic nude mice. This will be described in detail as part of the combination studies below. By performing immunohistochemistry for standard vascular markers (CD31 and CD34) followed by microvessel density

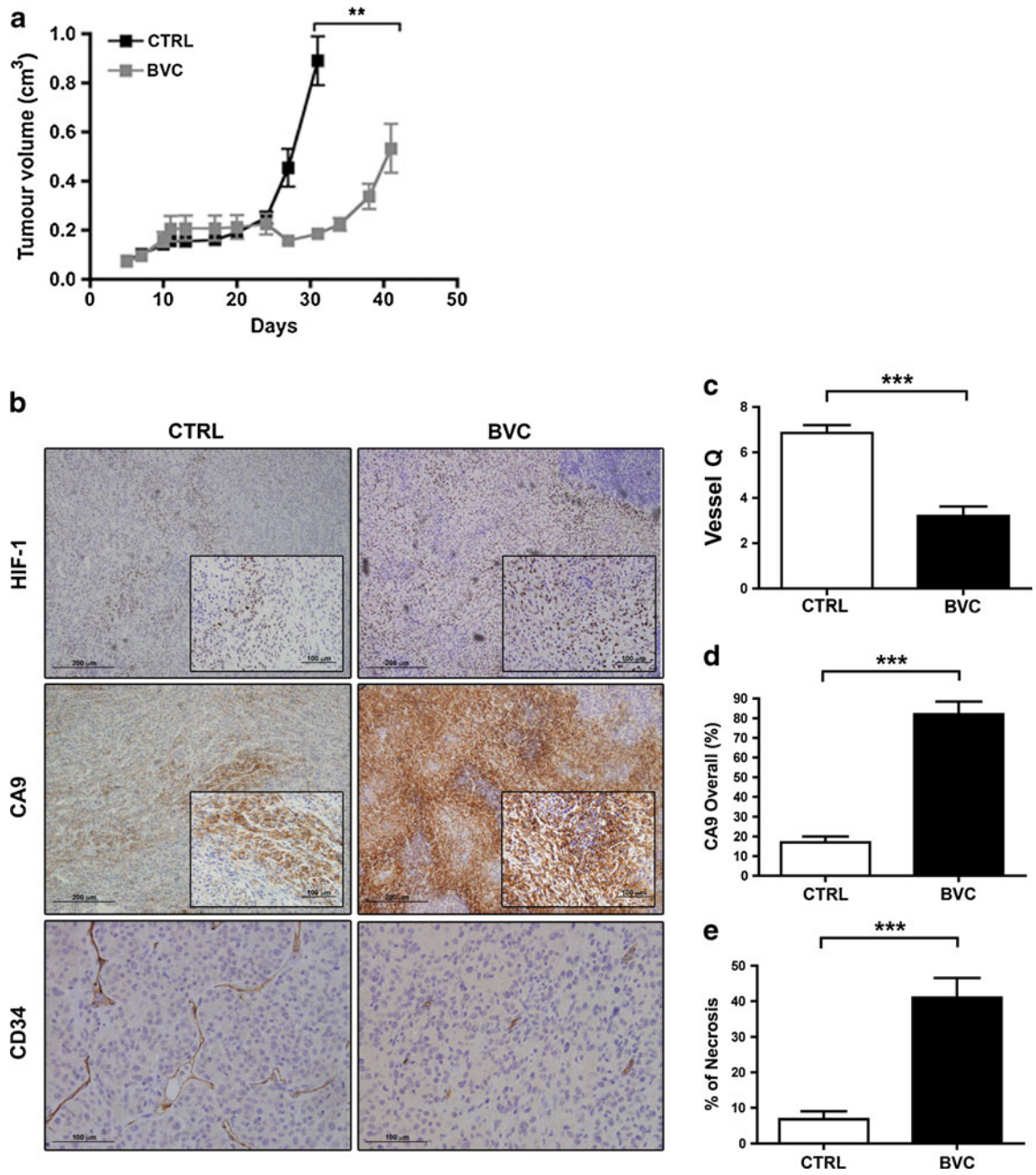

Fig. 1 Analysis of bevacizumab-treated U87-MG tumors. (*A*) Tumor growth of U87-MG in vivo, treated with bevacizumab (BVC) or vehicle control (CTRL), started from day 12 to the end of the experiment. mean±SE, $N=5$. *Double asterisk* (**) $P<0.01$. (*B*) Immunohistochemical staining of tumor sections from CTRL or BVC-treated tumors show increased hypoxia using HIF-1 and CA9, and a marker of vessel morphology using CD34. Main images are ×10 magnification and inset images ×20 magnification. Sections were stained and scored for (*C*) vessel Q (CD31), (*D*) CA9 levels, and (*E*) necrosis. Mean±SE. *Single asterisk* (*) $P<0.05$; *triple asterisk* (***) $P<0.001$

counting, we confirmed that resistant tumors exhibit a significantly sparser vasculature (Fig. 1). Therefore, therapeutic resistance does not appear to be primarily related to renewed vascularization due to a switch to alternative angiogenic growth factors, as shown in other models of bevacizumab resistance [7]. Expression of HIF-1α, as well as of carbonic anhydrase IX (CA9), a robust HIF target and well-established marker of hypoxia, was dramatically increased in the resistant tumors, indicating that their growth continued in a significantly more oxygen-depleted environment consistent with the data reported by Rapisarda et al. [8].

Molecular characterization of bevacizumab-resistance model

In order to gain a comprehensive understanding of the molecular processes that are associated with and potentially critical for the resistance process, total RNA from treated and non-treated tumors was subjected to expression analysis using HGU133plus2 Affymetrix arrays. The full data set for the Affymetrix array expression analysis is available at http://www.ncbi.nlm.gog/geo/query/acc.cgi?acc=GSE37956. A central theme in the bevacizumab-resistant tumors was the coordinated activation of the HIF-driven transcription program (Fig. 2). A large proportion of HIF targets exhibited coordinated upregulation, in most cases with more than one array probe. Notably, glycolytic HIF targets including aldolases A and C, triosephosphate isomerase 1, and 6-phosphofructo-2-kinase/fructose-2,6-biphosphatase 3, as well as the inducible glucose transporters GLUT1/SLC2A1 and GLUT3/SLC2A3, were robustly induced, pointing to an increased reliance on glycolytic utilization of glucose. In contrast, a significant repression in bevacizumab-resistant tumors was seen at the level of pyruvate dehydrogenase (PDH) alpha 1 and beta genes that govern the entry of pyruvate into the tricarboxylic acid (TCA) cycle [9]. PDH activity is inhibited by phosphorylation by pyruvate dehydrogenase kinases (PDK). PDK1 and PDK3 isoforms, which are well-documented HIF targets [10–12], were strongly upregulated in the bevacizumab-resistant tumors, further supporting a biochemical shift away from oxidative phosphorylation (OXPHOS) (Fig. 2). Arguably, the most striking gene expression change in bevacizumab-resistant tumors was the global downregulation of mitochondrial metabolism genes, in particular, members of all five mitochondrial OXPHOS complexes (Fig. 2). Finally, several components of the TCA cycle, including fumarate hydratase (FH) and succinate dehydrogenase (SDH) were downregulated (Fig. 2), which may contribute to tumor growth as they also function as tumor suppressors [13].

KEGG pathway analysis confirmed that energy metabolism represented one of the dominant changes associated with the bevacizumab-resistant tumors. Thus, glycolytic genes were most abundant among the upregulated genes, together with genes belonging to fructose and mannose metabolism, pentose phosphate pathway, amino sugar and nucleotide sugar metabolism, and inositol phosphate metabolism (Supplementary Table S1A). The hypergeometric and corrected hypergeometric p values were lower than 0.01 for all these pathways. Conversely, among the downregulated genes, OXPHOS was the top repressed pathway, with p values lower than 1.00E-28, with pyruvate metabolism and TCA cycle also exhibiting very highly significant repression (Supplementary Table S1B). An additional signature observed in the bevacizumab-resistant tumors was increased endoplasmic reticulum stress and unfolded protein response. In particular, the key mediators of these responses ATF4, 5, 6 and DDIT3/CHOP were all strongly overexpressed (Supplementary Table S2), consistent with our previous observations that more severe hypoxia developing during the course of antiangiogenic therapy activates non-HIF pathways [14].

In vitro effects of chronic hypoxia on mitochondrial OXPHOS gene expression

To investigate whether hypoxia represents the primary cause of the downregulation of mitochondrial respiration and Krebs cycle genes, we undertook a comprehensive in vitro survey of low oxygen effects in U87 cells. Interestingly, several OXPHOS genes and Krebs cycle components that were found downregulated in the arrays also responded by downregulation in hypoxia, including ATP5A1, ATP5G3, NDUFA9, FH, and MDH1 (Fig. 3). MRPL36 and MRPS11, two genes thought to be critical in the assembly of the OXPHOS complexes [15, 16], also showed downregulation in hypoxia, similar to the effect of bevacizumab (Fig. 3). However, the majority of the genes downregulated in the arrays failed to exhibit downregulation during hypoxic exposure, suggesting that other factors may be primarily responsible [17]. Reexamination of the arrays revealed that several transcription factors that regulate mitochondrial gene expression (including OXPHOS) were downregulated: NRF1, TFAM, and TFB2M [18–20] (Supplementary Table S3).

Exploitation of the increased glycolytic gap: in vivo synergism between bevacizumab and DCA

Based on the marked signature of increased HIF signaling and decreased mitochondrial OXPHOS, we hypothesized that the bevacizumab-resistant tumors would be particularly sensitive to mitochondrial reactivators. The top small molecule candidate from this class is DCA, which inhibits PDK activity, thereby increasing the flux of pyruvate into the mitochondria and promoting glucose oxidation over glycolysis [21, 22]. Taking into

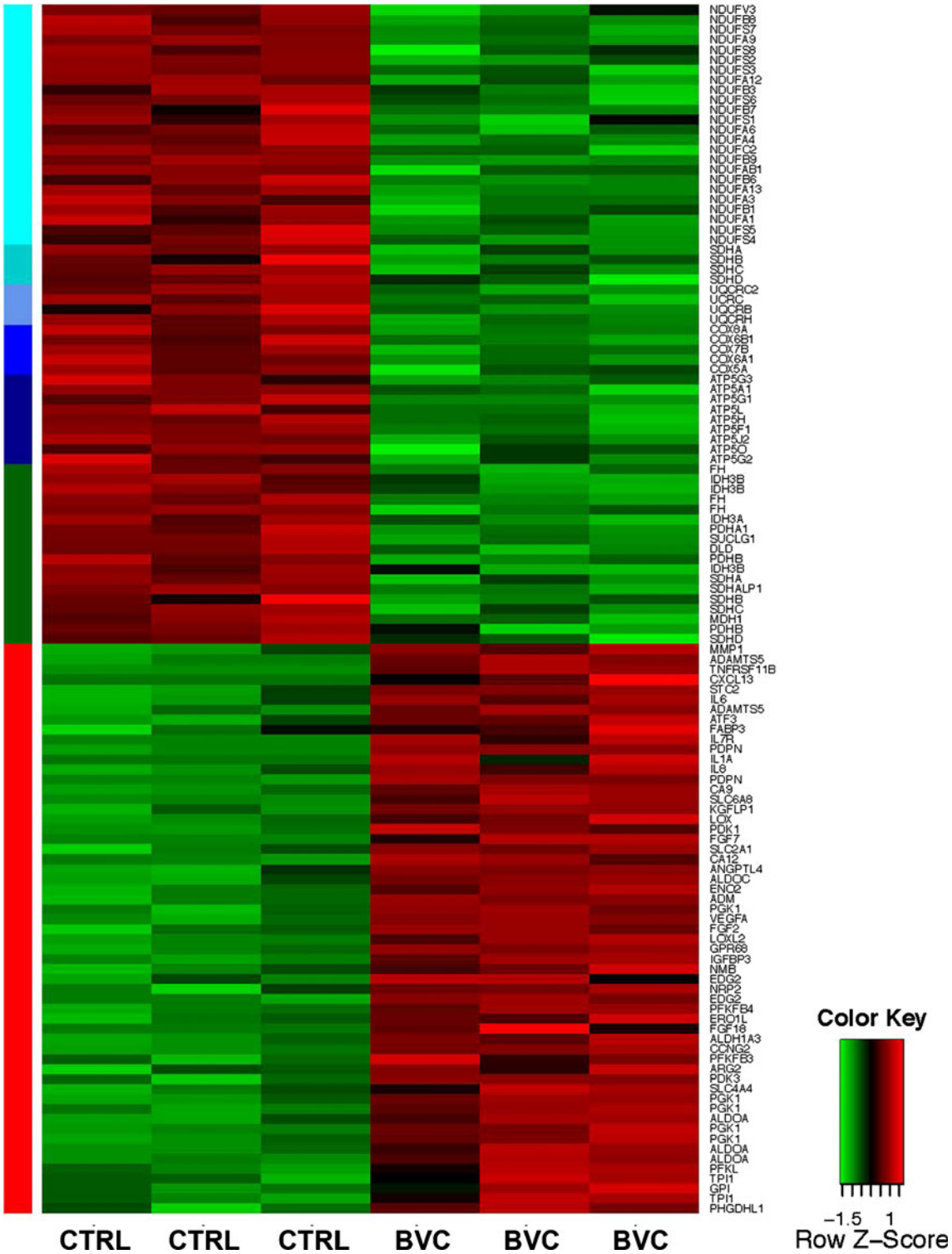

Fig. 2 Gene expression changes in control versus bevacizumab-treated groups. *X-axis* represents control and bevacizumab-treated tumors. Array data were preprocessed using GCRMA, normalized using quantile normalization and log base 2. Expression is shown standardized per gene (*Z* values; *color key at the top*). *Y-axis*: gene symbols shown on the *right*. *Blue bands on side* indicate mitochondrial gene complexes (from *light blue*=I to *dark blue*=V). *Green band* indicates Krebs cycle genes. *Red band* indicates HIF targets

account the well-recognized side effects of antiangiogenic therapy as well as of DCA, for the assessment of the drug combination, we chose a submaximal dose of the antiangiogenic agent (2.5 mg/kg; every 3 days by

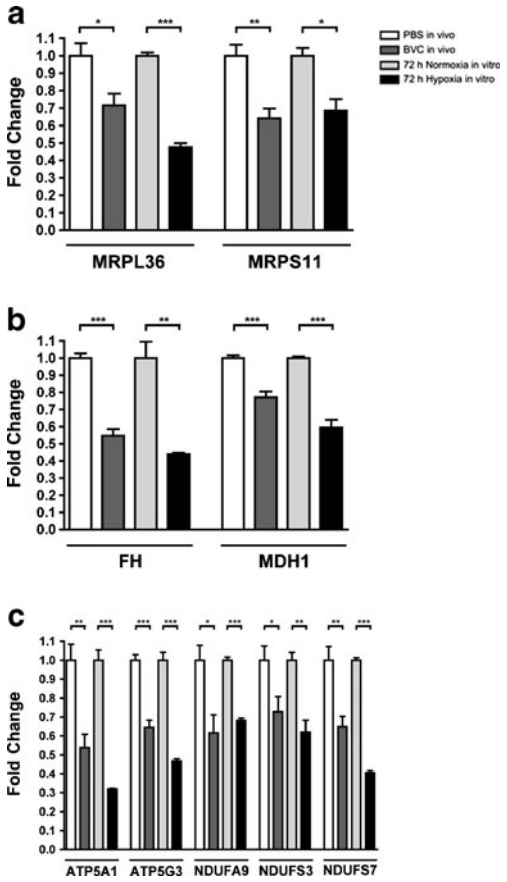

Fig. 3 Downregulation of metabolic mitochondrial genes in bevacizumab-resistant tumors. Quantitative PCR analysis was performed to investigate the effects of BVC treatment or hypoxia on U87 cells. For normoxia versus hypoxia comparisons, cells were incubated at 1 % oxygen for 72 h. The following mitochondrial genes were tested: (*A*) mitochondrial ribosomal genes, (*B*) Krebs cycle enzymes, and (*C*) electron transport complex I and V components. Gene levels are expressed as fold changes by comparison in vivo to PBS controls and in vitro to normoxic controls. Mean±SE. *Single asterisk* (*) $P<0.05$; *double asterisk* (**) $P<0.01$; *triple asterisk* (***) $P<0.001$

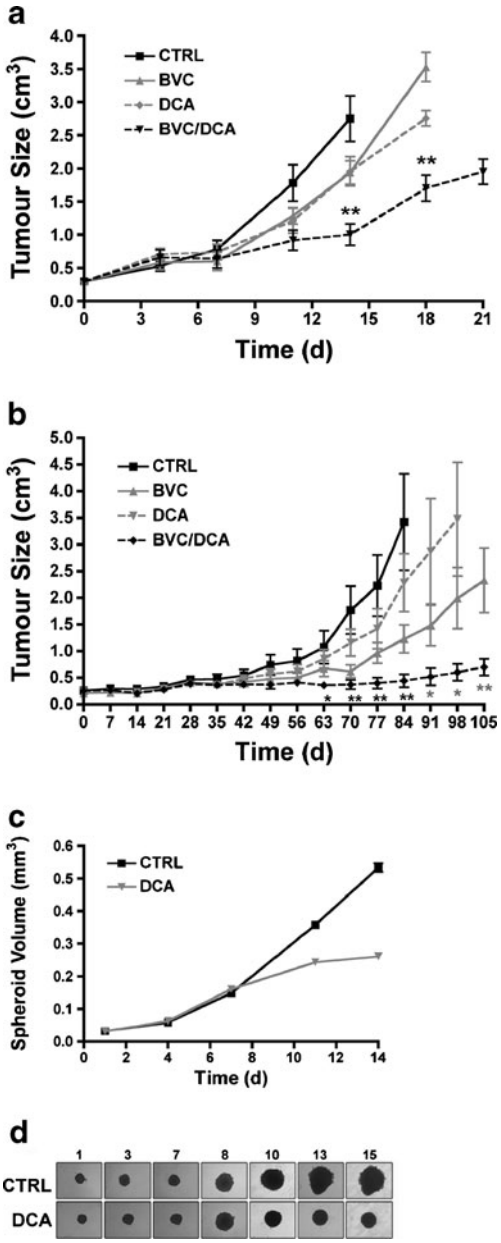

Fig. 4 DCA amplifies the effects of BVC on tumor growth in vivo. (*A*) Tumor growth of U87-MG in vivo, treated with either CTRL, BVC, DCA, or BVC/DCA, starting from day7 until the end of the experiment. Mean±SE, $N=4–6$. *Single asterisk* (*) $P<0.05$; (*B*) tumor growth of U118 in vivo, treated with either CTRL, BVC, DCA, or BVC/DCA. The U118 tumors were slow growing, and so, day0 is treatment start time. Mean±SE, $N=4–8$. *Single asterisk* (*) $P<0.05$; *double asterisk* (**) $P<0.01$; (*black stars* is comparison to CTRL, *gray stars* to BVC alone); (*C*) growth of U87-MG spheroids treated with either vehicle control (CTRL) or 10 mM DCA. Spheroids were allowed to grow to 0.2 mm^3 before being treated with DCA every 3 days. NB: error bars are small and within the symbols. (*D*) Pictures (at ×5 magnification) show representative images of the CTRL and DCA-treated spheroids

intraperitoneal injection), a strategy which is widely employed in vivo [23]. This approach is also anticipated to increase our ability to detect synergism between the two drugs, both from the standpoint of tumor response and effects on HIF signaling. Indeed, treatment with bevacizumab and DCA dramatically blocked tumor growth compared to each drug alone (Fig. 4*A* and Supplementary Fig. S1). In order to assess the generality of the response, we investigated an additional GBM cell type, U118. The response in U118-based grafts was also much more robust with the combination, compared to the individual drugs (Fig. 4*B* and Supplementary Fig. S1).

The efficacy of glycolytic inhibitors in overcoming resistance to bevacizumab has been previously proposed [24] without experimental confirmation. DCA and 2-DG were discussed together as part of this concept. However, when 2-DG was tested in parallel to DCA, no additive effect to

bevacizumab was noticed. This was despite the transient effect of 2-DG as a single agent, administered at the concentration described in the literature (Supplementary Fig. S2). Thus, mitochondrial reactivation and direct inhibition of glycolysis have different effects in combination with bevacizumab.

In vitro effects of DCA

Spheroid models provide a system of intermediate complexity between standard two-dimensional culture systems and tumors in vivo because of oxygen and nutrient gradients. Unlike monolayer systems, expanding spheroids mimic the increased avascularity of the in vivo structures growing in presence of bevacizumab. U87 spheroids were generated, as described [25], and grown for 7 days until they reached 0.2 mm^3. Spheroids of this size are large enough to allow diffusion of a drug across the spheroid but also are starting to form a small central area of hypoxia and display gradients of nutrients, pH and O_2. Robust divergence of the growth kinetics between DCA-treated and non-treated groups was noticed after 3 days of treatment. This effect was persistent, and from 6 days onward, DCA significantly compromised spheroid expansion (Fig. 4*C*, *D*).

Effect of bevacizumab and DCA combination on HIF targets and histological markers of tumor growth

In order to address whether the effect of the combination on tumor growth was primarily determined by increased cell death or decreased proliferation, we performed histological analyses on these tumors, using well-established markers. Necrosis was higher in the treated tumors compared to the untreated ones, but no significant difference was observed between the drugs alone or in combination (Fig. 5). Proliferation rate, as evaluated by quantification of Ki-67 (MIB-1) staining, was significantly lower in the combination group compared to both untreated and bevacizumab-only tumors, suggesting that the effect of the combination was predominantly cytostatic (Fig. 5). We, then, assessed the effects of the drug combination on HIF signaling, using a combination of immunohistochemistry/quantitative RT-PCR (Figs. 5, 6). Surprisingly, while known to increase oxygen consumption in various experimental systems, DCA alone was not sufficient to measurably increase the expression of the HIF targets in vivo. However, in combination with bevacizumab, CA9 expression increased dramatically in the viable U87 tumor cells. In U118, on the other hand, submaximal bevacizumab alone led to a dramatic increase in all HIF targets tested, without further measurable increase in the combination-treated tumors (Fig. 6 and Supplementary Fig. S3). However, the major caveat is that the tumors surviving in the presence of the combination were dramatically smaller and practically stationary, factors that should mitigate the extent of hypoxia.

Discussion

The main goal of our study was to gain a deeper understanding of tumor adaption to bevacizumab, by identifying pathways that are associated with resistance, with a particular focus on metabolic responses. We concentrated on a heterotopic rather than an orthotopic model, primarily to ensure the feasibility of monitoring neoplastic growth and escape. Additionally, as subcutaneous tumors reach significantly larger volumes than their orthotopic counterparts, they are arguably more relevant for modeling advanced and hypoxic malignancies.

In a recently published orthotopic model of GBM, increased hypoxia post-bevacizumab has been reported [24, 26]; however, investigating long-term growth differences is less feasible in such systems. Despite the "classic" status of tumor metabolism in cancer research and its recent revival, no drug that acts primarily at this level has been approved for routine clinical use [27]. DCA, a small molecule which crosses the blood brain barrier [22], showed promising results in a clinical trial in GBM in combination with surgery, temozolomide, and radiation [21], with multiple additional trials currently underway http://clinicaltrials.gov/ct2/results?term=+Dichloroacetate). However, the effect of DCA as a single agent is transient at best, and our tumor models certainly reflect this limitation. A recent study discussed the possibility that bevacizumab treatment should sensitize tumors to both 2-DG and DCA [24], but these predictions have been confirmed only for DCA in our hands. The lack of a measurable additive or synergistic effect of 2-DG was unlikely due to biological inactivity or inadequate dosing as it was transiently effective as a single agent. Questions remain as to the mechanism of DCA-mediated tumor inhibition in the presence of bevacizumab. While DCA was reported to block angiogenesis by itself [21], measurement of mean vessel density did not confirm this in our system.

DCA has been shown to exhibit increased cytotoxic effects under hypoxia in a variety of cell lines [28]. The current paradigm is that DCA accelerates oxygen consumption by mitochondrial reactivation and further decreases local oxygen tension [29], thus posing an additional challenge on tumor cells to survive and/or proliferate. Moreover, it has been demonstrated that in cells "hardwired" to selectively utilize glycolysis for ATP generation due to mitochondrial DNA

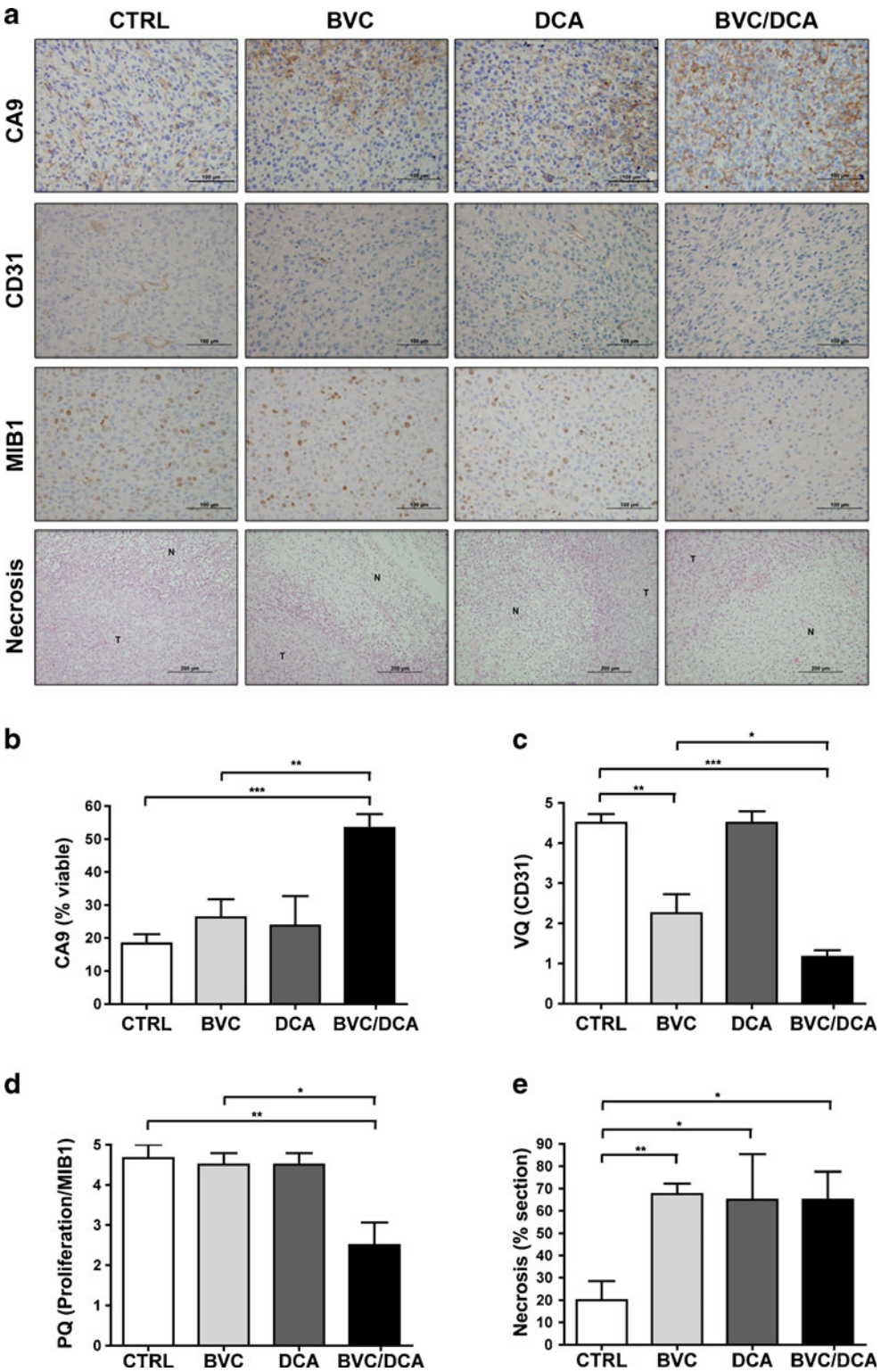

Fig. 5 Effect of bevacizumab and DCA on U87-MG tumor histology. (*A*) Immunohistochemical staining for CA9, CD31, Ki-67 (MIB-1), and necrosis in FFPE sections of U87-MG tumor xenografts treated with BVC, DCA, a combination of BVC and DCA, or vehicle control (CTRL). Quantification of (*B*) percentage of the viable tissue positive for CA9; (*C*) vessel score, VQ, (CD31); (*D*) proliferation index, PQ, (Ki-67); and (*E*) necrosis. All images are shown at ×20 magnification. Mean±SE. *Single asterisk* (*) $P<0.05$; *double asterisk* (**) $P<0.01$; *triple asterisk* (***) $P<0.001$

mutations, forced OXPHOS induced by DCA had a toxic effect. DCA also exhibits synergistic cytotoxicity in vitro in combination with cisplatin and topotecan, two antineoplastic agents known to damage mitochondrial DNA [30]. One could speculate that the downregulation of mitochondrial genes in the bevacizumab-resistant tumors represents a form of mitochondrial dysfunction that sensitizes to the effects of DCA.

Interestingly, the effect of DCA, as a single agent, on HIF targets in xenografts was subtle at best despite its

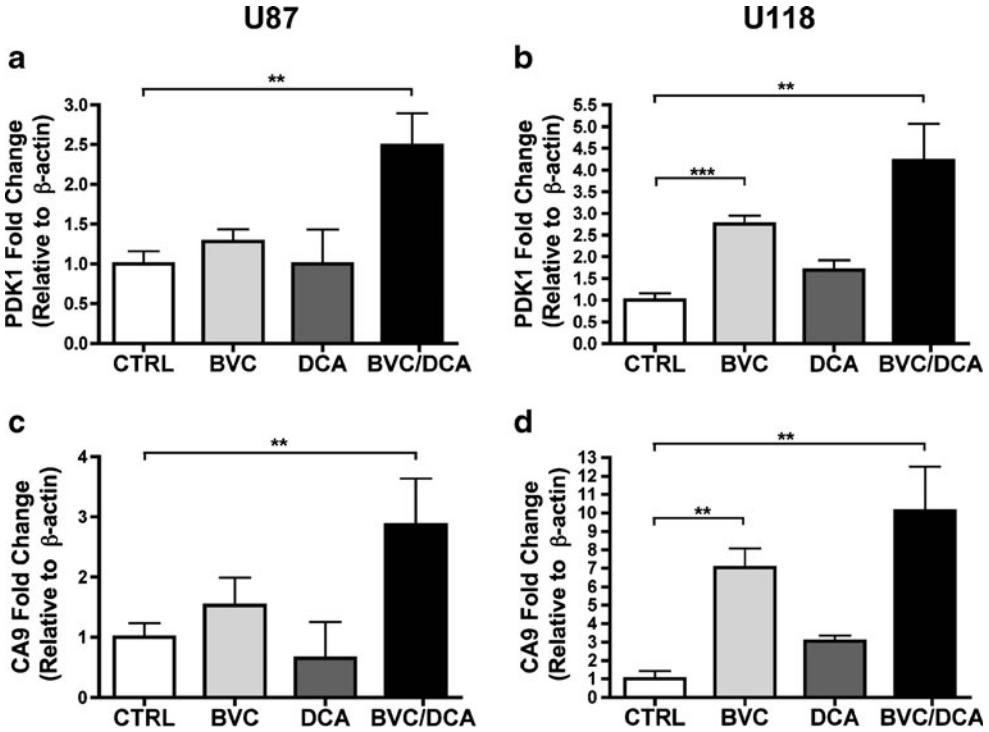

Fig. 6 Effect of combination therapy of bevacizumab and DCA on key metabolic genes. Quantitative PCR analysis was performed to investigate the effects of CTRL, BVC, DCA, or BVC/DCA treatment on U87-MG and U118 tumors by measuring fold changes in the RNA (*A* and *B*) PDK1 (*C* and *D*) CA9. Mean±SE, *N*=4–8. *Single asterisk* (*) $P<0.05$; *double asterisk* (**) $P<0.01$; *triple asterisk* (***) $P<0.001$

well-recognized positive effect on oxygen consumption. In contrast, together with bevacizumab, DCA led to increased expression of most HIF targets tested in the surviving tumors versus bevacizumab alone. A possible explanation for these results is that forced OXPHOS induced by DCA in the presence of very low levels of oxygen may lead to increased reactive oxygen species production, which, in turn, may contribute to additional induction of HIF [31]. Additionally, or alternatively, DCA in the presence of bevacizumab may lead to a further decrease in the local oxygen concentration to levels where the induction of HIF targets becomes more evident by quantitative RT-PCR assay. In addition to increased CA9 expression, enhanced expression of the HIF targets PDK1, 3 and GLUT1 was observed in the tumors surviving in the presence of the drug combination in either U87 or U118 cells. This may reflect a more dramatic "last resort" metabolic shift critical for tumor cell survival. In particular, increased expression of PDK1/3 may be part of a "final attempt" by the tumor cells to counteract in part the effect of DCA and inactivate mitochondrial OXPHOS. Such metabolic shifts in tumors surviving in the presence of bevacizumab plus DCA may also provide important clues on how to further increase the efficacy of this combination. For example, one could speculate that the resistant tumors may exhibit at least some sensitivity to a further escalation of DCA concentration although toxicity of this compound may become a limiting factor. Upregulation of tumor-specific CA9 may also play an important role in the survival of the combination-treated tumors as it accelerates the elimination of excess CO_2 generated from the reactivation of the Krebs cycle [25]. Therefore, CA9 inhibitors which have recently shown promising anticancer effects [32, 33] may be regarded as realistic candidates for a third component of a combination strategy.

In conclusion, molecular dissection of tumor adaptation to anti-VEGF agents may offer valuable clues for building more efficient combinations that include targeting cancer metabolism.

Author's contributions Conception and design: M.I. and A.L.H. Acquisition of data: K.K., S.W., H.E.G., H.T., J.L., J.S., A.L.S., R.L., D.S., C.M.D., and M.H. Analysis and interpretation of data: M.I. and A.L.H. Writing, review, and/or revision of the manuscript: M.I. and A.L.H. Administrative, technical, or material support: F.B. Study supervision: M.I. and A.L.H.

Funding source The work was supported by grants from Cancer Research United Kingdom [S.W., A.L.H., H.T., R.L., J.L.], METOXIA p-Medicine European Union Framework 7 [D.S., F.B.], Rhodes Scholar [H.G.], Indiana University Cancer Center startup funds, and American Cancer Society [M.I., C.M.D., K.K.].

Conflict of interest No potential conflicts of interest to declare.

References

1. Cao Y, Arbiser J, D'Amato RJ, D'Amore PA, Ingber DE, Kerbel R, Klagsbrun M, Lim S, Moses MA, Zetter B et al (2011) Forty-year journey of angiogenesis translational research. Sci Transl Med 3:114rv3
2. Wick W, Wick A, Weiler M, Weller M (2011) Patterns of progression in malignant glioma following anti-VEGF therapy: perceptions and evidence. Curr Neurol Neurosci Rep 11:305–312
3. Raizer JJ, Grimm S, Chamberlain MC, Nicholas MK, Chandler JP, Muro K, Dubner S, Rademaker AW, Renfrow J, Bredel M (2010) A phase 2 trial of single-agent bevacizumab given in an every-3-week schedule for patients with recurrent high-grade gliomas. Cancer 116:5297–5305
4. Bergers G, Hanahan D (2008) Modes of resistance to anti-angiogenic therapy. Nat Rev Cancer 8:592–603
5. Friedman HS, Prados MD, Wen PY, Mikkelsen T, Schiff D, Abrey LE, Yung WK, Paleologos N, Nicholas MK, Jensen R et al (2009) Bevacizumab alone and in combination with irinotecan in recurrent glioblastoma. J Clin Oncol 27:4733–4740
6. Winter SC, Shah KA, Campo L, Turley H, Leek R, Corbridge RJ, Cox GJ, Harris AL (2005) Relation of erythropoietin and erythropoietin receptor expression to hypoxia and anemia in head and neck squamous cell carcinoma. Clin Cancer Res Off J Am Assoc Cancer Res 11:7614–7620
7. Davies S, Dai D, Pickett G, Thiel KW, Korovkina VP, Leslie KK (2011) Effects of bevacizumab in mouse model of endometrial cancer: defining the molecular basis for resistance. Oncol Rep 25:855–862
8. Rapisarda A, Hollingshead M, Uranchimeg B, Bonomi CA, Borgel SD, Carter JP, Gehrs B, Raffeld M, Kinders RJ, Parchment R et al (2009) Increased antitumor activity of bevacizumab in combination with hypoxia inducible factor-1 inhibition. Mol Cancer Ther 8:1867–1877
9. Harris RA, Bowker-Kinley MM, Huang B, Wu P (2002) Regulation of the activity of the pyruvate dehydrogenase complex. Adv Enzyme Regul 42:249–259
10. Wigfield SM, Winter SC, Giatromanolaki A, Taylor J, Koukourakis ML, Harris AL (2008) PDK-1 regulates lactate production in hypoxia and is associated with poor prognosis in head and neck squamous cancer. Br J Cancer 98:1975–1984
11. Kim JW, Tchernyshyov I, Semenza GL, Dang CV (2006) HIF-1-mediated expression of pyruvate dehydrogenase kinase: a metabolic switch required for cellular adaptation to hypoxia. Cell Metab 3:177–185
12. Lu CW, Lin SC, Chen KF, Lai YY, Tsai SJ (2008) Induction of pyruvate dehydrogenase kinase-3 by hypoxia-inducible factor-1 promotes metabolic switch and drug resistance. J Biol Chem 283:28106–28114
13. Frezza C, Pollard PJ, Gottlieb E (2011) Inborn and acquired metabolic defects in cancer. J Mol Med (Berl) 89:213–220
14. Rzymski T, Milani M, Pike L, Buffa F, Mellor HR, Winchester L, Pires I, Hammond E, Ragoussis I, Harris AL (2010) Regulation of autophagy by ATF4 in response to severe hypoxia. Oncogene 29:4424–4435
15. Prestele M, Vogel F, Reichert AS, Herrmann JM, Ott M (2009) Mrpl36 is important for generation of assembly competent proteins during mitochondrial translation. Mol Biol Cell 20:2615–2625
16. Emdadul Haque M, Grasso D, Miller C, Spremulli LL, Saada A (2008) The effect of mutated mitochondrial ribosomal proteins S16 and S22 on the assembly of the small and large ribosomal subunits in human mitochondria. Mitochondrion 8:254–261
17. Tang X, Lucas JE, Chen JL, Lamonte G, Wu J, Wang MC, Koumenis C, Chi JT (2012) Functional interaction between responses to lactic acidosis and hypoxia regulates genomic transcriptional outputs. Cancer Res 72:491–502
18. Scarpulla RC (2002) Nuclear activators and coactivators in mammalian mitochondrial biogenesis. Biochim Biophys Acta 1576:1–14
19. Falkenberg M, Gaspari M, Rantanen A, Trifunovic A, Larsson NG, Gustafsson CM (2002) Mitochondrial transcription factors B1 and B2 activate transcription of human mtDNA. Nat Genet 31:289–294
20. Larsson NG, Barsh GS, Clayton DA (1997) Structure and chromosomal localization of the mouse mitochondrial transcription factor A gene (*Tfam*). Mamm Genome 8:139–140
21. Michelakis ED, Sutendra G, Dromparis P, Webster L, Haromy A, Niven E, Maguire C, Gammer TL, Mackey JR, Fulton D et al (2010) Metabolic modulation of glioblastoma with dichloroacetate. Sci Transl Med 2:31ra34
22. Michelakis ED, Webster L, Mackey JR (2008) Dichloroacetate (DCA) as a potential metabolic-targeting therapy for cancer. Br J Cancer 99:989–994
23. Pechman KR, Donohoe DL, Bedekar DP, Kurpad SN, Hoffmann RG, Schmainda KM (2011) Characterization of bevacizumab dose response relationship in U87 brain tumors using magnetic resonance imaging measures of enhancing tumor volume and relative cerebral blood volume. J Neurooncol 105:233–239
24. Keunen O, Johansson M, Oudin A, Sanzey M, Rahim SA, Fack F, Thorsen F, Taxt T, Bartos M, Jirik R et al (2011) Anti-VEGF treatment reduces blood supply and increases tumor cell invasion in glioblastoma. Proc Natl Acad Sci U S A 108:3749–3754
25. Swietach P, Patiar S, Supuran CT, Harris AL, Vaughan-Jones RD (2009) The role of carbonic anhydrase 9 in regulating extracellular and intracellular ph in three-dimensional tumor cell growths. J Biol Chem 284:20299–20310
26. de Groot JF, Fuller G, Kumar AJ, Piao Y, Eterovic K, Ji Y, Conrad CA (2010) Tumor invasion after treatment of glioblastoma with bevacizumab: radiographic and pathologic correlation in humans and mice. Neuro Oncol 12:233–242
27. Kaelin WG Jr, Thompson CB (2010) Q&A: cancer: clues from cell metabolism. Nature 465:562–564
28. Anderson KM, Jajeh J, Guinan P, Rubenstein M (2009) In vitro effects of dichloroacetate and CO2 on hypoxic HeLa cells. Anticancer Res 29:4579–4588
29. Chen Y, Cairns R, Papandreou I, Koong A, Denko NC (2009) Oxygen consumption can regulate the growth of tumors, a new perspective on the Warburg effect. PLoS One 4:e7033
30. Stockwin LH, Yu SX, Borgel S, Hancock C, Wolfe TL, Phillips LR, Hollingshead MG, Newton DL (2010) Sodium dichloroacetate selectively targets cells with defects in the mitochondrial ETC. Int J Cancer 127:2510–2519
31. Park JH, Kim TY, Jong HS, Kim TY, Chun YS, Park JW, Lee CT, Jung HC, Kim NK, Bang YJ (2003) Gastric epithelial reactive oxygen species prevent normoxic degradation of hypoxia-inducible factor-1alpha in gastric cancer cells. Clin Cancer Res Off J Am Assoc Cancer Res 9:433–440
32. Dubois L, Peeters S, Lieuwes NG, Geusens N, Thiry A, Wigfield S, Carta F, McIntyre A, Scozzafava A, Dogne JM et al (2011) Specific inhibition of carbonic anhydrase IX activity enhances the in vivo therapeutic effect of tumor irradiation. Radiother Oncol 99:424–431
33. Morris JC, Chiche J, Grellier C, Lopez M, Bornaghi LF, Maresca A, Supuran CT, Pouyssegur J, Poulsen SA (2011) Targeting hypoxic tumor cell viability with carbohydrate-based carbonic anhydrase IX and XII inhibitors. J Med Chem 54:6905–6918